Chapter 1

Introduction & Literature Survey

1.1 Background

Understanding and predicting turbulent flow is vital for a wide range of applications, from weather prediction to car design. The phenomena that are observed in turbulent flows, such as the beautiful and intricate eddy structures, are also fascinating. Turbulence is characterized by its disorder or apparent unpredictability. It typically has a large range of length and time scales: in atmospheric turbulence the eddies may range in size from centimetres up to hundreds of kilometres. The rapidly changing velocity field in turbulent flows encourages rapid mixing which enhances diffusion of momentum, mass and heat. This feature can be advantageous if one wants to remove heat or mix fluids, or it can be disadvantageous if, for instance, one wants to minimize friction drag. Turbulence is also dissipative, meaning that energy must be constantly supplied to the flow in order for turbulence to be maintained or else it will decay (a commonly cited example being the motion of stirred liquid in a cup, where the fluid eventually ceases moving). This dissipation of turbulent kinetic energy is linked to an "energy cascade", where energy is supplied to the largest eddies by shearing motions in the bulk flow, which interact with and transfer energy to smaller eddies. In the smallest eddies the velocity gradients are largest and viscous action converts kinetic energy into heat. Whilst it is influenced by the fluid viscosity and density, turbulence is not a material property of the fluid but a continuum flow phenomena (continuum in the sense that the minimum length scale in a turbulent flow is always much greater than the mean free path of its constituent molecules). The turbulence considered in this thesis is also three-dimensional. Turbulence can occur in 2-D but it exhibits behaviour unlike 3-D turbulence, in particular the energy cascade seems to work in reverse, leading to larger and larger eddies.

Turbulent flow predictions have evolved significantly during the last half-century, largely due to the appearance of digital computers in the 1950's and 60's, and their exponential increase in processing power over the following decades. Before the advent of computing, predictions were made using either empirical correlations or integral methods. The latter approach involves the solution of ordinary differential equations (in 2-D flows) through the use of integral parameters such as momentum thickness and skin-friction coefficient (by assuming profiles or shape functions, see for example [1]).

This approach is limited to fairly simple flows which do not involve boundary-layer separation or recirculation, but is still commonly used in industry [2].

At present, there are five main approaches to predicting turbulent flow. The first and conceptually the simplest approach is to solve directly the equations governing fluid flow, the Navier-Stokes equations. This so-called "Direct Numerical Simulation" (DNS) has the advantages of not needing any assumptions of the turbulence behaviour and hence data from DNS is often used in a similar manner to experimental results (the bonus being that quantities that cannot be determined experimentally can easily be examined, as all flow parameters are calculated). In fact it has even been used to estimate the measurement errors in experiments (see, for example, Moin & Mahesh [3]). DNS is also proving useful for examining the internal mechanisms of turbulence and transition from laminar to turbulent flow. The disadvantage of DNS is the computational expense: massively parallel computers have to be used and computations are limited to relatively low-Reynolds-number flows with a small ratio of large to small eddies. This high cost is due to the nature of turbulence itself. In order for turbulence to be represented accurately it is necessary to resolve *all* the length and time scales of the flow. Tennekes & Lumley [4] showed that the computational cost scales with the cube of the integral-scale Reynolds number, Re_l^3. It is therefore unlikely that DNS will be used routinely in engineering calculations for the foreseeable future, although it is invaluable as a tool for providing very detailed data which may be used to help develop or to validate turbulence models.

The second approach, Large Eddy Simulation (LES), uses a coarser grid than that employed in DNS and applies the filtered Navier-Stokes equations (effectively N-S equations averaged over a small region of space). Since the grid cannot discern the smallest scales of turbulence, a sub-grid-scale model is used to account for the dissipation of energy at the smallest scales and any "backscatter" of energy from the small to the large scales. The large-scale motions, which are responsible for most of the transport of momentum and turbulence energy, are computed explicitly and do not require modelling. Therefore, it is anticipated that this method should be more accurate than the RANS approach discussed below, in which all turbulent scales are modelled. LES was first developed for application to weather prediction, but is increasingly being used throughout the engineering and scientific communities. However, the relatively high computational expense still limits LES to analysis and trouble-shooting rather than as an aid to engineering design[1].

The third approach uses Reynolds-Averaged Navier-Stokes (RANS) equations. Here the turbulent flow is considered as consisting of two components: a fluctuating part and a mean or average part. The mean flow is calculated using RANS equations which are obtained by averaging the Navier-Stokes equations over time, space or using ensemble averaging. The equations look very similar to the unaveraged (instantaneous) Navier-Stokes equations but for an additional non-linear term involving the Reynolds stress, $\overline{u_i u_j}$ (where u_i is the fluctuating velocity and the overbar denotes Reynolds averaging). A transport equation can also be derived for the unknown Reynolds stress, but this involves

[1]For example, at present in UMIST an opposed wall-jet flow is being examined using both LES and RANS approaches. The RANS simulations (using a two-equation model) take approximately 6 hours whereas the LES simulations take between 1 and 2 weeks, on the same platform, depending on grid resolution.

additional unknown third-order terms ($\overline{u_i u_j u_k}$). Likewise, the expression for $\overline{u_i u_j u_k}$ involves unknown fourth moments and so on. This issue of specifying the Reynolds stress is known as the turbulence modelling "closure problem". The closure problem is also complicated by the fact that the Reynolds stress may depend upon non-local events. In the exact equation for $\overline{u_i u_j}$ there are terms involving the fluctuation pressure, p, for which one can derive a Poisson equation. This equation can be solved, using Green's functions, but the value of p at any point in the flow is found to be a function of the velocity at all points throughout the whole flow domain. "Single-point" closures assume that the Reynolds stress can be calculated in terms of local parameters. Various single-point turbulence models exist which attempt to approximate $\overline{u_i u_j}$, ranging from simple algebraic expressions to additional transport equations for each of the six independent Reynolds stresses. These models are discussed below (Section 1.2).

Solving the RANS equations with a single-point linear eddy-viscosity model (discussed below) can be thought of as solving the Navier-Stokes equations for a laminar flow (i.e. the mean velocity) but with a modified fluid viscosity which is a function of the local turbulence behaviour. If the flow is stationary (i.e. if the averaged velocity field does not change over time) it is not necessary to compute the time-dependent flow behaviour with a RANS scheme, unlike DNS or LES where the flow must always be considered as unsteady. Symmetry can also be used to reduce the computational demands where appropriate so, for example, the axisymmetric impinging jet studied in this thesis was treated as essentially a 2-*D* problem. DNS and LES on the other hand require full 3-*D* solutions in order to model 3-*D* turbulence. The RANS approach using single-point closure is therefore economical and flexible and is widely used in industry for both design and analysis.

The fourth method of analyzing turbulent flows involves "multi-point" or in most cases simply "two-point" correlations. Here the turbulent statistics at two separate points in space are used. The analysis is complex and the resulting equations are sometimes intractable. Research is principally being undertaken by two groups, L'Ecole Centrale de Lyon and the Los Alamos National Laboratories. Complex turbulent flows have been examined using two-point closures, but only in relatively simple geometries. Whilst this approach is unlikely to be used in practical engineering applications in the near future, the theories developed in two-point closures give insight into some of the physics of turbulent interactions and provide guidance for the development of single-point turbulence models.

The fifth and final approach to predicting turbulent flow uses Probability Density Functions (PDFs). A PDF expresses the likelihood of an event taking place per unit sample space[2]. The mean velocity and Reynolds stress are the first and second moments of the Eulerian PDF of velocity. Therefore, if the shape of the PDF can be determined then the closure problem can be solved. An equation for the velocity PDF can be derived from the Navier-Stokes equations. In this equation the convective transport and the mean pressure gradient term are in closed form but the remaining fluctuating pressure and viscous terms require modelling. Various models for the PDF equation are detailed by Pope

[2]For example, if there is a uniform probability of velocity, V, being greater than one and less than three metres per second (i.e. an equal chance that V will take any value between 1 and 3 m/s), then the PDF will be a constant value of $1/2$ between $V = 1$ and $V = 3$.

[5]. This method has mostly been applied to reactive flows because it avoids the need for additional closure approximations in the chemical reaction equations. For simpler non-reactive flows, the current PDF models involving particle methods lead to increased computing times compared to single-point Reynolds-stress models. As yet, there have not been sufficient comparative studies between PDF and Reynolds-stress models to draw any firm conclusions as to their relative accuracy.

For simplicity, the above discussion has been limited to the five main approaches to predicting turbulent flow. There are numerous other hybrid methods in which, for example, an unsteady RANS calculation is used near solid boundaries while LES is applied in the bulk of the flow (an approach dubbed "Detached Eddy Simulation", DES). An interesting discussion of hybrid methods (including DES, VLES and URANS) is provided by Spalart [6].

The objective of the work presented in this thesis is to develop a new wall boundary condition suitable for simulations using RANS equations and single-point Reynolds-stress models (the third of the above five approaches). The following sections review single-point Reynolds-stress models, near-wall flow phenomena and current approaches used in modelling the near-wall flow behaviour.

1.2 Turbulence modelling

The Reynolds-averaged continuity and momentum equations can be written in Cartesian coordinates as follows:

$$\frac{\partial \rho}{\partial t} + \frac{\partial}{\partial x_j}(\rho U_j) = 0 \tag{1.1}$$

$$\frac{\partial}{\partial t}(\rho U_i) + \frac{\partial}{\partial x_j}(\rho U_i U_j) = -\frac{\partial P}{\partial x_i} + \frac{\partial}{\partial x_j}\left[\mu\left(\frac{\partial U_i}{\partial x_j} + \frac{\partial U_j}{\partial x_i}\right) + \lambda\delta_{ij}\frac{\partial U_m}{\partial x_m} - \rho\overline{u_i u_j}\right] \tag{1.2}$$

where upper-case U_i and P denote Reynolds-averaged velocity and pressure, ρ is the density, μ is the molecular viscosity, λ is the bulk viscosity and δ_{ij} is the Kronecker delta. Expanding the above expressions in three-dimensions gives 4 equations (continuity and three momentum equations) and 10 variables: three velocity components (U, V and W), pressure and six independent Reynolds stress components[3]. To close this system of equations, an expression for the Reynolds stress needs to be found. Boussinesq, in the late nineteenth century, approached the turbulence closure problem by assuming the turbulent stress to be proportional to the strain rate, introducing an apparent or "eddy" viscosity as the scalar proportionality term. The turbulence closure problem therefore changed from calculating six Reynolds stresses to finding one eddy-viscosity. One of the simplest approaches to calculating this eddy-viscosity has been the mixing length model which was derived independently by G. I. Taylor [7] and L. Prandtl [8]. Here, the following expression is obtained for the eddy-viscosity in a simple shear flow in which $\partial U/\partial y$ is the only strain-rate:

$$\nu_t = l_m^2 \left|\frac{\partial U}{\partial y}\right| \tag{1.3}$$

[3]There are only six independent components, since $\overline{u_i u_j}$ is a symmetric tensor ($\overline{u_i u_j} = \overline{u_j u_i}$).

The mixing length, l_m, is a characteristic of the local flow and is prescribed algebraically. There are no additional transport equations to solve and so the mixing length model is referred to as an algebraic or zero-equation model. The problem is now a question of how to prescribe the mixing length, l_m. In the fully-turbulent region of equilibrium boundary layers, l_m can be described by a simple linear expression, $l_m = \kappa y$, where y is the distance from the wall and κ the von Kármán constant. However, in more complex flows l_m must be varied considerably to obtain good experimental agreement. Another limitation of the simple mixing length model is that it predicts that the turbulent viscosity vanishes when the strain rate $(\partial U/\partial y)$ is zero, as may occur for example in separated boundary layers, whereas in reality the effects of turbulence can be significant in such regions.

A slightly more sophisticated class of models involves the solution of a transport equation for a turbulence parameter. Prandtl's one-equation model [9] solves a transport equation for the turbulent kinetic energy, k, so that the eddy-viscosity is given by:

$$\nu_t = c_\mu k^{1/2} l \tag{1.4}$$

where c_μ is a constant and l is a prescribed length scale. In this model, the problem associated with turbulent viscosity becoming zero where the velocity takes a maximum or minimum value is overcome by using $k^{1/2}$ as a velocity scale. However, as with the zero-equation models, its weakness is the algebraic length scale prescription: a different algebraic expression needs to be applied for different flow geometry. A more recent one-equation model by Spalart & Allmaras [10] which solves a transport equation directly for ν_t has been quite successful in predicting attached flow around airfoils [11]. However, it performs less well in separated flows and the model requires the prescription of a wall-distance which can be difficult to specify around a body of complex geometry.

Two-equation eddy-viscosity models involve the solution of transport equations for two turbulence parameters (usually turbulent kinetic energy and a second independent variable). This enables the calculation of the velocity and length scales which are used to calculate the eddy-viscosity. There have been many two-equation models using a variety of different choices for the second variable (e.g. ε, kl, ω, ω^2, τ). The most popular scheme for the last 20 years has been the $k-\varepsilon$ model. The "standard" version of the model was presented by Jones & Launder [12] with improved values for constants and damping functions given later by Launder & Sharma [13]. In the $k-\varepsilon$ model the eddy-viscosity is calculated from:

$$\nu_t = c_\mu \frac{k^2}{\varepsilon} \tag{1.5}$$

where c_μ is a constant of proportionality, which is normally defined empirically by considering flow under local equilibrium. The quantity ε is the rate of dissipation of turbulent kinetic energy per unit mass, which appears directly in the k-equation as a sink term. The dissipation rate can be thought of physically as the speed at which turbulent kinetic energy is transferred from large scale eddy-motion to smaller scales (since the rate of dissipation by the small eddies is equal to the rate of energy transfer from the large eddies). An exact equation for the transport of ε can be derived from

the definition of the dissipation rate[4] but the expression includes many unknown terms, including double and triple correlations of fluctuating velocity, pressure and velocity gradients (see, for example [14]). The modelled ε-equation of Launder & Sharma was therefore devised more by intuition and empirical reasoning, following the earlier work of Chou [15], Davidov [16] and Harlow & Nakayama [17]. Reasonably accurate solutions have been obtained using the $k-\varepsilon$ model for a wide range of industrially relevant flows.

Another popular two-equation model solves a transport equation for the "turbulence frequency" or, more correctly, the dissipation rate per unit turbulent kinetic energy, ω, as the second parameter[5]. This approach was first suggested by Kolmogorov [18] and in more recent times the major proponent of the $k-\omega$ model has been Wilcox. In his book [14], Wilcox discusses the performance of $k-\varepsilon$ and $k-\omega$ models with reference to free shear flows, boundary layers and separated flows and reports that the $k-\omega$ model performs well in 2-*D* boundary layers with adverse or favourable pressure gradients and in recirculating flows, but suffers from increased sensitivity to freestream boundary conditions in free shear flows. Since the dissipation rate, ε, tends to a finite value at the wall and k falls to zero, ω $(=\varepsilon/k)$ tends to infinity. To overcome this problem, wall boundaries are handled by prescribing the value of ω at the first node adjacent to the wall. For a review of one and two-equation models see, for example, Pope [5] or Patel *et al*. [19].

Menter [20] adopted a pragmatic approach to two-equation modelling, taking the best aspects of both $k-\varepsilon$ and $k-\omega$ models and blending the two. In the Shear Stress Transport (SST) model, the $k-\omega$ model is applied in the inner region of the boundary layer (near the wall) whilst the $k-\varepsilon$ model is used in the outer region and in free shear flows, to remove the $k-\omega$ model's dependence upon freestream turbulence levels. The expression for eddy-viscosity is also modified to make the shear stress proportional to the kinetic energy in the boundary layer. Two blending functions, which employ the distance from the wall, are used to switch between the turbulence models and to modify μ_t. The SST model has been demonstrated to perform well in a variety of flows including adverse pressure-gradient boundary layers and transonic flows.

Whilst linear eddy-viscosity models are, in general, relatively easy to implement and give reasonable predictions of attached boundary layer flows, they have a number of limitations. In simple shear flows where the velocity $U=U(y)$, the normal Reynolds stresses predicted by a linear EVM are isotropic (i.e. $\overline{u^2}=\overline{v^2}=\overline{w^2}=2k/3$) whereas experiments and DNS studies [21] indicate that there is normal stress anisotropy with $0.5\overline{u^2}\approx\overline{v^2}\approx\overline{w^2}$. Whilst this may not be influential in correctly predicting the dynamic field in a simple shear flow, Brundrett & Baines [22] showed that the correct prediction of normal stress anisotropy is vital in predicting secondary flow in non-circular ducts. In impinging flows, linear models which have the turbulent kinetic energy production proportional to the strain-rate squared $\left(P_k\propto S^2\right)$ overpredict the turbulent kinetic energy near the stagnation point and

[4]The dissipation rate of turbulent kinetic energy is defined as: $\varepsilon=\nu\overline{\frac{\partial u_i}{\partial x_k}\frac{\partial u_i}{\partial x_k}}$.

[5]One can transform the modelled ε-equation into the ω-equation by re-tuning the constants and introducing an additional cross-diffusion term. This source term can be derived from the definition $(\omega=\varepsilon/k)$ and expanding $(D\varepsilon/Dt=\omega Dk/Dt+kD\omega/dt)$ using the transport equations for k and ω.

therefore predict far higher heat transfer rates than occur experimentally (see discussion in Chapter 5). In addition, a linear model predicts a linear variation in swirl velocity with radius in a fully-developed swirling shear flow in a pipe, although experiments [23] indicate that the profile is non-linear. Likewise, the asymmetric velocity profile that is observed in a fully-developed curved channel flow cannot be predicted with a linear EVM without curvature corrections [24].

More sophisticated Differential Stress Models (DSMs), also called Second-Moment Closures or Stress-Transport Models, are able to overcome this inability to account properly for rotational strains and the inaccurate prediction of normal stress anisotropy. These models involve the solution of transport equations for each of the independent Reynolds stress components. The transport equations for the Reynolds stress are of the following form:

$$\frac{D\overline{u_i u_j}}{Dt} = P_{ij} + d_{ij} + \varepsilon_{ij} + \phi_{ij} \tag{1.6}$$

where terms on the right-hand-side are respectively: production, P_{ij}, diffusion, d_{ij}, dissipation, ε_{ij}, and a term known as the "pressure-strain" or "redistribution", ϕ_{ij}. The production term is calculated in its exact form and does not require modelling. The effect of the pressure-strain term is to redistribute energy among the normal stresses whilst usually acting as a sink for the shear stresses. Because ϕ_{ij} has zero trace, it does not appear in the turbulent kinetic energy equation used in simpler two-equation models (which is derived from the transport equation for $\overline{u_i u_j}$). In addition to improved modelling of flow curvature and Reynolds stress anisotropy, DSM's are able to account for the history of the Reynolds stresses, which is important in rapidly developing flows. For example, in an initially anisotropic turbulence field which has its mean strain-rate suddenly set to zero, two-equation models predict an instantaneous return to isotropy whereas experiments (and differential stress models) predict a more gradual change. A review of recent developments in differential stress models is given by leading researchers in [25]. Whilst these models offer the greatest sophistication of current one-point closures, they are costly to use, requiring the solution in 3-D of 11 transport equations rather than the 6 used by two-equation models. Moreover, the models are complex to implement and computations can sometimes suffer from numerical instability.

Non-linear Eddy-Viscosity Models (NLEVMs) have been developed as a compromise between the simple low-cost linear schemes and the more accurate but expensive DSMs. In a NLEVM, the Reynolds stress is calculated from an algebraic expression which includes linear, quadratic and sometimes higher-order combinations of strain-rate (S) and vorticity (Ω). A number of approaches have been adopted in developing NLEVMs. The first method takes a Differential Stress Model and simplifies the transport equations for the Reynolds stress using the "weak equilibrium assumption" [26]:

$$\frac{D}{Dt}\overline{u_i u_j} = \frac{\overline{u_i u_j}}{k}\frac{Dk}{Dt} + \underbrace{k\frac{D}{Dt}\left(\frac{\overline{u_i u_j}}{k}\right)} \tag{1.7}$$

where D/Dt represents combined convection and diffusion and the underbraced term is assumed zero.

This results in an implicit Algebraic Stress Model (ASM) in which the Reynolds stress appears on both sides of an expression involving non-linear functions of strain and vorticity. Different methods have been used to obtain an explicit formula (in the form $\overline{u_i u_j} = f(S, \Omega)$), see for example Gatski & Speziale [27] or Apsley & Leschziner [28]. An alternative more pragmatic approach to developing NLEVMs is simply to introduce higher-order combinations of S and Ω into the eddy-viscosity model and then tune the constants for a wide range of flows. This approach was formalised by Pope [29] and has been used by, among others, Craft *et al*. [30] and Speziale [31]. Some further approaches to deriving NLEVM's have involved Renormalization-Group (RNG) theory [32] and Direct Interaction Approximation (DIA) methods [33]. Quadratic combinations of S and Ω are necessary in NLEVMs to account for Reynolds stress anisotropy while swirl and curvature effects are only accounted for by cubic terms (for details, see Suga [34]). Some models have also incorporated constraints such as realizability, for instance Speziale's quadratic model [31] which ensures that turbulent kinetic energy is always positive. In general, NLEVM's solve transport equations for two or three turbulence parameters and so, in terms of computing costs, these models are marginally more expensive than linear two-equation EVMs but far less than DSMs. NLEVMs are unable to account accurately for history effects (since convection and diffusion of the individual Reynolds stress components are not modelled directly) but nevertheless these models have been shown to perform reasonably well in a wide variety of complex flows [34, 35].

Finally, it should be mentioned that different RANS turbulence models can be combined to make two-layer or zonal schemes. Typically a two-equation or higher-order model is used in the bulk of the flow while the near-wall region is treated with a simpler, usually algebraic or one-equation, low-Reynolds-number model. For example, the zonal model of Iacovides & Launder [36] employed a $k-\varepsilon$ model in the high-*Re* region and a van Driest mixing-length model close to walls to study the flow around pipe bends. The two-layer approach can offer savings in computing times compared to integrating a high-order model all the way to the wall surface, but there can be problems coupling the two layers in complex flows and results depend upon the location of the boundary.

1.3 Near-Wall Flow Phenomena

There is a vast amount of literature on the statistics and structure of turbulence near solid boundaries (see, for example, the review article of Moin & Mahesh [3]). The object of the present discussion is not to review this literature but merely to identify what it is about turbulent flow in the near-wall region that causes problems for turbulence modelling and to introduce some basic terminology describing the near-wall flow. The section begins by deriving the universal "laws of the wall", which describe the near-wall velocity and temperature profiles for flows close to equilibrium, after which some analytical and DNS results for the behaviour of Reynolds stresses near walls are discussed. The distance from the wall in these discussions is specified in terms of wall units or y^+ values. This is defined for simple

shear flows, where $U = U(y)$, as follows:

$$y^+ = \frac{U_\tau y}{\nu} \qquad\qquad U_\tau = \sqrt{\frac{\tau_{wall}}{\rho}} \tag{1.8}$$

where U_τ is the "friction velocity", τ_{wall} is the wall shear stress and y is the distance from the wall.

Law of the Wall for Velocity

In a zero-pressure-gradient fully-developed Couette flow in which there are no streamwise gradients of velocity or stress, the wall-normal velocity is zero from continuity and the equation for the streamwise mean U-velocity simplifies to:

$$\frac{\partial}{\partial y}\left(\mu\frac{\partial U}{\partial y} - \rho\overline{uv}\right) = 0 \tag{1.9}$$

Integrating this using the wall boundary conditions $-\rho\overline{uv} = 0$ and $\tau = \mu\partial U/\partial y = \tau_{wall}$ at $y = 0$, one obtains:

$$\mu\frac{\partial U}{\partial y} - \rho\overline{uv} = \tau_{wall} \tag{1.10}$$

In the thin region immediately adjacent to the wall ($y^+ < 5$), termed the "viscous sublayer", the Reynolds stress ($\rho\overline{uv}$) is negligible in comparison to the viscous stress ($\mu\partial U/\partial y$). Integrating Equation (1.10) with ($\rho\overline{uv} = 0$) leads to an expression in which the U-velocity is a linear function of the wall-normal distance. This is often written:

$$U^+ = y^+ \tag{1.11}$$

where U^+ is the dimensionless streamwise velocity given by $U^+ = U/U_\tau$. As one moves further away from the wall, viscous effects diminish and the turbulent stress dominates. In the fully turbulent region, from $y^+ \approx 30$ to $y/\delta \approx 0.1$ (where δ is the boundary layer thickness), viscous stresses are negligible in comparison to the turbulent stresses and Equation (1.10) simplifies to:

$$-\rho\overline{uv} = \tau_{wall} \tag{1.12}$$

Applying the mixing length hypothesis:

$$-\rho\overline{uv} = \rho l_m^2\left(\frac{\partial U}{\partial y}\right)^2 \tag{1.13}$$

assuming an equilibrium length scale, $l_m = \kappa y$, and integrating, leads to the following expression:

$$U^+ = \frac{1}{\kappa}\ln y^+ + C \tag{1.14}$$

The above formula is known as the "log-law". The two constants κ and C are usually assigned the following values for a smooth wall:

$$\kappa = 0.41 \qquad\qquad C = 5.0$$

However, values of κ and C given in turbulence modelling literature vary by approximately $\pm 8\%$. The linear and log-layers described by Equations (1.11) and (1.14) are shown in Figure 1.1 on semi-logarithmic axes. Between the two regions is a buffer zone (from approximately $y^+ = 5$ to 30) where the turbulence levels increase and viscous effects diminish with wall-distance. The combined linear and log-laws are often collectively termed the "law of the wall" and the whole region from the wall up to the outer edge of the log-law is called the "inner-layer". Beyond this region, further from the wall, is the "outer layer". Here the velocity-defect law is held to apply. This states that the difference between the mean velocity and the free-stream velocity normalized by the friction velocity, $(U_\infty - U)/U_\tau$, is a function only of dimensionless wall-distance (y/δ) and is independent of the fluid properties. However, unlike the linear and log-laws, the velocity in the outer region is flow dependent and a "universal" defect law does not exist.

Millikan [37] used an alternative approach to derive the law of the wall where the velocity profile in the viscous sublayer was assumed to be solely a function of the wall-distance (y), the wall shear stress (τ_{wall}) and fluid properties (ρ and μ), and not directly dependent upon the boundary layer thickness (δ) or the free-stream velocity, (U_∞). Dimensional arguments were then used to arrive at Equation (1.11). A similar approach can be taken in the log-layer, where the flow is considered to be independent of fluid properties, U_∞ and δ. The log-law has also recently been derived using Rapid Distortion Theory (RDT) [38].

The existence of the law of the wall has been confirmed by numerous experiments and by DNS simulations of zero pressure-gradient boundary layers [21] and channel flows [39, 40]. The discrepancy in the values of the constants used in the log-law may be because of low-Reynolds-number effects, experimental "noise" or perhaps because the log-law is being assumed to apply over too wide a portion of the flow. Both Spalart [21] and Moser *et al*. [40] when presenting their DNS data discuss the stringent criteria for a true log-law region. Moser *et al*. also assess some claims [41] that in fact the log-law is more correctly a power-law profile. Bradshaw & Huang [42] discuss in some detail the performance of the log-law in boundary layers in which there are strong streamwise pressure gradients. They argue that simply modifying the constants to be functions of the local shear stress (τ) or its gradient $(\partial\tau/\partial y)$ is unlikely to produce a generally-applicable wall model, although they also note that the log-law appears "tenacious" in providing reasonable results for non-equilibrium flows in which its underlying assumptions are no longer valid. Some authors have employed a more sophisticated characterization of the various regions than the simple approach presented above. For example Pope [5] identifies in total seven overlapping regions.

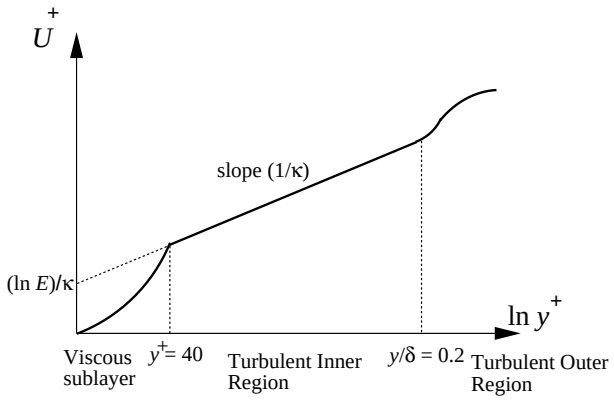

Figure 1.1: Schematic "universal" velocity distribution for a smooth wall (boundary values shown are approximate).

Law of the Wall for Temperature

Following on from the law of the wall for velocity there is a similar law for temperature. The temperature, T, is made dimensionless by the "friction" temperature, T_τ, and wall temperature, T_{wall}:

$$T^+ = \frac{(T_{wall} - T)}{T_\tau} \qquad\qquad T_\tau = \frac{q_{wall}}{\rho c_p U_\tau} \tag{1.15}$$

In the viscous-dominated sublayer, the relationship between T^+ and y^+ is given by Fourier's heat-conduction law:

$$q_{wall} = -\lambda \frac{\partial T}{\partial y} \tag{1.16}$$

which can be reformulated as:

$$T^+ = y^+ \sigma \tag{1.17}$$

where σ is the molecular Prandtl number ($\sigma = \mu c_p/\lambda$) – the ratio of a fluid's ability to diffuse momentum to its ability to diffuse heat. Further from the wall a log-law for temperature can be derived of the following form (see Cebeci & Bradshaw[43]):

$$T^+ = \frac{1}{\kappa_h} \ln\left(y^+\right) + c_h \tag{1.18}$$

where the constants are given by:

$$\kappa_h = \kappa/\sigma_t \qquad\qquad c_h = \frac{1}{\kappa_h} \ln(E) + P\left(\frac{\sigma}{\sigma_t}\right) \tag{1.19}$$

and the Jayatilleke [44] P-function is given by:

$$P\left(\frac{\sigma}{\sigma_t}\right) = 9.24\left[\left(\frac{\sigma}{\sigma_t}\right)^{3/4} - 1\right]\left\{1 + 0.28\exp\left[-0.007\left(\frac{\sigma}{\sigma_t}\right)\right]\right\} \tag{1.20}$$

The quantity σ_t is the turbulent Prandtl number (defined in analogy to the molecular Prandtl number with $\sigma_t = \mu_t c_p/\lambda_t$). Usually, the log-law for temperature is expressed:

$$T^+ = \sigma_t\left[U^+ + P\left(\frac{\sigma}{\sigma_t}\right)\right] \tag{1.21}$$

The temperature log-law is applicable in near-equilibrium flows from $y^+\sigma \approx 50$ to $y/\delta_t \approx 0.1$, where δ_t is the thickness of the thermal boundary layer. Compared to the velocity-law, the log-law for temperature appears more sensitive to streamwise pressure gradients [42].

Near-Wall Reynolds Stress Behaviour

Immediately adjacent to the wall, the behaviour of the Reynolds stresses, k and ε can be obtained from the asymptotic behaviour of the fluctuating velocity components, as follows:

$$\overline{u^2} = \overline{a_1^2}y^2 + 2\overline{a_1 a_2}y^3 + \left(\overline{a_2^2} + 2\overline{a_1 a_3}\right)y^4 + \ldots \tag{1.22}$$

$$\overline{v^2} = \overline{b_2^2}y^4 + \ldots \tag{1.23}$$

$$\overline{w^2} = \overline{c_1^2}y^2 + 2\overline{c_1 c_2}y^3 + \left(\overline{c_2^2} + 2\overline{c_1 c_3}\right)y^4 + \ldots \tag{1.24}$$

$$\overline{uv} = \overline{a_1 b_2}y^3 + \left(\overline{a_1 b_3} + \overline{a_2 b_2}\right)y^4 + \ldots \tag{1.25}$$

where the a's, b's and c's are functions of x, z and time but not of y. Due to continuity, the wall-normal fluctuating velocity component, v, dies out faster than the wall-parallel components, u and w, hence the wall-normal stress $\overline{v^2}$ increases with y^4 whilst the two wall-parallel components $\overline{u^2}$ and $\overline{w^2}$ increase as y^2. The turbulent kinetic energy, k, is given by:

$$\begin{aligned} k &= \frac{1}{2}\left(\overline{u^2} + \overline{v^2} + \overline{w^2}\right) \\ &= \frac{1}{2}\left[\left(\overline{a_1^2} + \overline{c_1^2}\right)y^2 + 2\left(\overline{a_1 a_2} + \overline{c_1 c_2}\right)y^3 + \ldots\right] \end{aligned} \tag{1.26}$$

and the dissipation rate, ε:

$$\begin{aligned} \varepsilon &= \nu\overline{\left(\frac{\partial u}{\partial y}\right)^2} + \nu\overline{\left(\frac{\partial v}{\partial y}\right)^2} + \nu\overline{\left(\frac{\partial w}{\partial y}\right)^2} \\ &= \nu\left[\left(\overline{a_1^2} + \overline{c_1^2}\right) + 4\left(\overline{a_1 a_2} + \overline{c_1 c_2}\right)y + \ldots\right] \end{aligned} \tag{1.27}$$

The dissipation rate is therefore finite at the wall ($\varepsilon = \nu\left(\overline{a_1^2} + \overline{c_1^2}\right)$ when $y = 0$). Referring back to the expression for k at the wall (Equation 1.26), the first-order terms result in the following expression for ε in terms of k:

$$\varepsilon = \nu\left(\overline{a_1^2} + \overline{c_1^2}\right) = \frac{2\nu k}{y^2} \tag{1.28}$$

At the wall surface, the dissipation rate of turbulence energy is balanced by viscous diffusion of kinetic energy towards the wall, which can be expressed:

$$\nu\frac{\partial^2 k}{\partial y^2} = \nu\frac{\partial^2\left[\left(\overline{a_1^2} + \overline{c_1^2}\right)y^2/2\right]}{\partial y^2} = \frac{2\nu k}{y^2} \tag{1.29}$$

An approximate profile for the near-wall turbulent kinetic energy production, P_k, in a zero pressure-gradient boundary layer can also be identified, as follows: in the log-layer, the shear stress is approximately constant across the near-wall region and since the strain-rate decreases as $\partial U/\partial y \propto y^{-1}$, the production-rate of kinetic energy ($P_k = \rho\overline{uv}\partial U/\partial y$) must be decreasing as the distance from the wall increases. Since $\overline{uv}$ is zero at the wall surface this means that the production-rate must reach a maximum value at some location between the wall and the log-layer. This inflection point occurs when:

$$\frac{\partial}{\partial y}\left(\rho\overline{uv}\frac{\partial U}{\partial y}\right) = 0 \tag{1.30}$$

Expanding this and substituting in Equation (1.10) it is possible to show that P_k reaches a maximum value when:

$$\mu\frac{\partial U}{\partial y} = -\rho\overline{uv} \tag{1.31}$$

i.e. when the viscous and turbulent stresses are equal. This point occurs in the buffer zone, between the linear and logarithmic regions identified above.

Detailed near-wall profiles of the Reynolds stresses, k and ε, have been obtained by DNS studies [21, 39, 40]. Profiles of the turbulence intensities, u', v' and w' from Moser *et al.* [40] for a channel flow at three different Reynolds numbers are reproduced in Figure 1.2. The largest component, the streamwise u', reaches a peak at approximately $y^+ = 13$ before decreasing sharply towards the wall. The anisotropy between the three normal Reynolds stresses is also shown. Figure 1.3, taken from Mansour *et al.* [45], shows the budget of the turbulent kinetic energy equation in a channel flow for $y^+ < 150$. Away from the wall ($y^+ > 30$) the turbulence is well approximated by the assumption of local equilbrium ($P_k = \rho\varepsilon$). As the wall is approached ($y^+ < 30$), viscous and turbulent diffusion terms increase and finally at the wall surface there is a balance between dissipation and viscous diffusion of k (as expressed above by Equations 1.28 and 1.29).

In order to discern the rapid changes in turbulence parameters across the near-wall region, as shown by the DNS results, it is clearly necessary to have a refined near-wall grid with a number of nodes within the viscous sublayer. The alternative would be to use empirically-based shape functions to represent the changes in velocity, temperature and turbulence parameters near the wall. In the

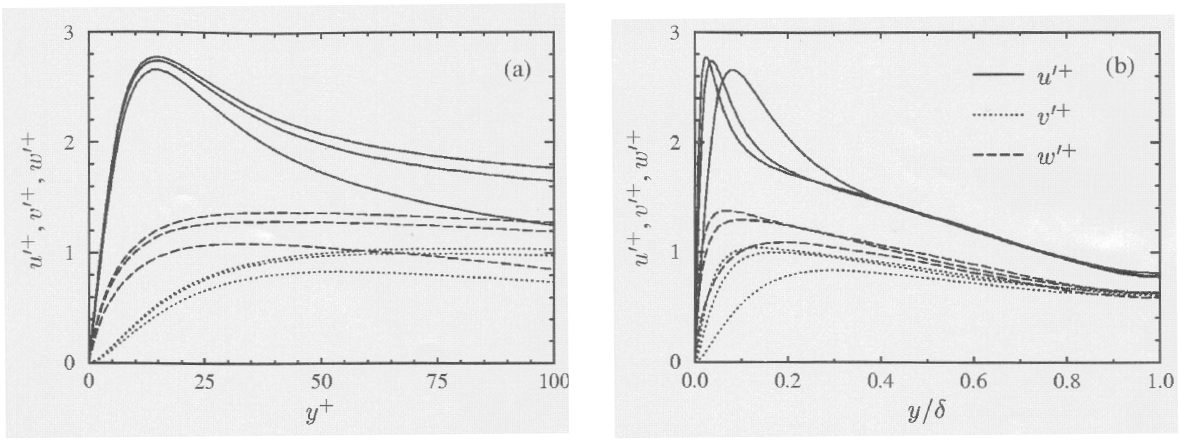

Figure 1.2: DNS predictions of the turbulence intensity across a fully-developed channel flow from Moser *et al*. [40] in wall coordinates (left) and global coordinates (right). Profiles for three Reynolds numbers are shown: $Re_\tau = U_\tau \delta/\nu = 590$, 395 and 180 (where U_τ is the friction velocity and δ the channel half-width). The peak RMS velocities generally increase with Reynolds number.

following section the implications of near-wall grid refinement are discussed along with the issue of computational costs and the need for effective wall functions.

1.4 Wall Functions vs. Low-*Re* Models

In RANS simulations of turbulent flows, there are two main approaches to the treatment of the near-wall region: the low-Reynolds-number approach and the wall-function approach. In the low-*Re* approach, specially formulated low-Reynolds-number turbulence transport equations are solved across the near-wall region. These incorporate damping functions that account for the increasing influence of molecular viscosity and the preferential damping of wall-normal fluctuating velocity components as the wall is approached. A very fine grid has to be employed[6] in order to track the rapid changes in the turbulence parameters near the wall, with typically 10 nodes within $y^+ = 10$ and the near-wall node below $y^+ = 1$. Provided that the turbulence model accounts correctly for the flow behaviour, this approach offers the greater accuracy of the two methods. However, the highly elongated cells in the near-wall region slow numerical convergence, CPU costs are high and computer storage requirements are large. The low-*Re* approach is therefore not routinely used for large and complex industrially-relevant CFD simulations.

The popular alternative is the high-*Re* approach which uses a coarse near-wall mesh so that the cell adjacent to the wall includes all of the viscous sublayer and part of the fully-turbulent region of the boundary layer (typically at the near-wall node $30 < y^+ < 300$). Transport equations solved in the main (high-*Re*) region of the flow domain therefore neglect the effects of molecular viscosity.

[6]To obtain an idea of the physical thickness of the viscous sublayer: for flow over a flat plate at a distance of one metre from the leading edge with a flow speed of 10ms^{-1} (21mph) the friction velocity is $u_\tau \approx 0.44\text{ms}^{-1}$ and the physical wall-normal height corresponding to $y^+ = 5$ is: $y_n = 0.17$mm. (c.f. Rautaheimo & Siikonen [46]).

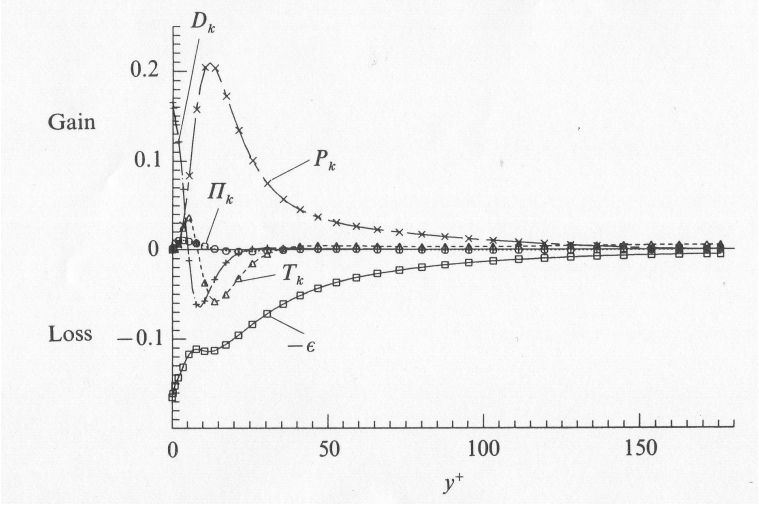

Figure 1.3: Channel flow turbulent kinetic energy equation budget taken from the DNS of Mansour *et al*. [45] for a Reynolds number, $Re = U_c\delta/\nu = 3,300$ (where U_c is the centreline velocity and δ the channel half-width). P_k = production; T_k = turbulent transport; D_k = viscous diffusion; ε_k = dissipation rate; Π_k = velocity pressure-gradient term.

In the cells adjacent to solid boundaries, empirically-based expressions (so-called "wall functions") are employed to obtain quantities such as wall shear stress which account for the influence of low-Reynolds-number effects on the flow near the wall. This approach is economical, both in computer storage and CPU time, with computations at least an order-of-magnitude faster than with the low-*Re* approach. However, the empirical profiles of velocity, turbulence parameters and temperature which are used in standard wall functions are only applicable in very simple near-wall flows and can lead to major errors in complex, non-equilibrium flows. In addition, the near-wall grid cannot be successively refined, since it is usually required to keep the near-wall node within the log-law region, and results can be sensitive to the size of the wall-adjacent cell.

A number of attempts have been made over the last 30 years to generalize wall functions for non-equilibrium flows. In the most basic wall function, the "universal" log-laws described in Section 1.3 are adopted for the wall-parallel velocity and temperature. Values of the turbulence parameters are specified at the near-wall node, based on local-equilibrium assumptions[7]. One of the first improvements upon this treatment, proposed by Launder & Spalding [48], was to replace the wall shear stress, τ_{wall}, in the velocity log-law with the turbulent kinetic energy, k (scaling the velocity with $k^{1/2}$ instead of the "friction velocity", $(\tau_{wall}/\rho)^{1/2}$, is crucial in flows involving separation, stagnation and reattachment, where the wall shear stress vanishes). The turbulent kinetic energy equation in the near-wall cell was solved using cell-averaged production and dissipation rates which were calculated by assuming constant shear stress and a linear turbulent length scale variation $\left(k^{3/2}/\varepsilon \propto y\right)$ across the near-wall

[7]For instance: $k = U_\tau^2/c_\mu^{1/2}$ and $\varepsilon = U_\tau^3/\kappa y$, based on an assumed constant shear stress $\left(\tau = -\rho\overline{uv} = c_\mu^{1/2}k\right)$ and equilibrium length scale $l = k^{3/2}/\varepsilon = c_l y$ (c.f. Grotjans & Menter [47]).

cell. However, even in fairly simple flows (fully-developed channel or pipe flow) the shear stress is not constant. Chieng & Launder [49] therefore proposed a wall function in which the near-wall cell was divided into two layers: the viscous sublayer and the fully turbulent region. In the viscous sublayer the shear stress, $\rho\overline{uv}$, was assumed to be zero and the turbulent kinetic energy to vary quadratically with wall distance, whilst in the fully turbulent region both $\rho\overline{uv}$ and k were assumed to vary linearly. Since at the wall the dissipation rate is given by $\varepsilon = 2\nu\left(\partial k^{1/2}/\partial y\right)^2$ and k varies quadratically, ε was assumed to take a uniform value in the viscous sublayer. In the fully turbulent region, ε was obtained from assuming an equilibrium turbulence length scale variation, $k^{3/2}/\varepsilon = c_l y$ (these profiles are discussed in detail in Chapter 2, see in particular Figures 2.2 and 2.3). The k-equation was solved in the near-wall cell using cell-averaged production and dissipation rates, and the dissipation rate, ε, was specified at the near-wall node. In order to locate the boundary of the viscous sublayer, the Chieng & Launder wall function assumed that the turbulence Reynolds number at the edge of the sublayer was $R_v = y_v k^{1/2}/\nu = 20$. For flows involving strong pressure gradients where the shear stress falls rapidly with wall distance, a constant value of $R_v = 20$ under-predicts the actual width of the sublayer. Johnson & Launder [50] therefore introduced a variable viscous sublayer thickness, based on the ratio of the diffusion of k towards the wall to the rate of dissipation within the sublayer. More recently, Ciofalo & Collins [51] proposed making the sublayer thickness a function of the local turbulence intensity. A review of the Launder & Spalding, Chieng & Launder and Johnson & Launder wall functions can be found in Acharya *et al*. [52] for flow past a surface-mounted 2-*D* rib. Performance characteristics of the three treatments were mixed and depended upon the turbulence model used ($k-\varepsilon$, algebraic stress or non-linear $k-\varepsilon$).

Two wall functions were proposed by Amano [53]. In the first, similar assumptions were adopted to the earlier treatments, but instead of solving only the k-equation in the near wall cell and prescribing the nodal value of ε based on local-equilibrium assumptions, Amano suggested solving transport equations for both k and ε in the near-wall cell using cell-averaged source and sink terms. The second wall function proposed by Amano used a three-layer model, in which different profiles for k and shear stress were used in the viscous sublayer, buffer layer and fully turbulent region. Better results were obtained using the three-layer model in an abrupt pipe expansion at various Reynolds numbers. A further proposal by Grotjans & Menter [47] assumed that the location of the wall, as specified by the user, was treated as the edge of the viscous sublayer. This enabled unlimited near-wall grid refinement. Wilcox [14, 54] presented two wall functions for the $k-\omega$ model. The first was analogous to a simple $k-\varepsilon$ wall function but the second included pressure-gradient terms which Wilcox suggested were necessary in order to obtain grid-independent results for flows with non-zero pressure gradients. Viegas & Rubesin [55] extended the Chieng & Launder wall function for compressible flow problems and, later, Viegas *et al*. [56] extended the treatment to enable greater flexibility of the near-wall node location: an approximate solution of the energy equation was obtained in the near-wall cell to determine the local temperature and density profiles and an additional power-law term was added into the logarithmic velocity profile expression to account for wake effects. Results using Viegas *et al*. wall

function were, for the most part, in good agreement with low-*Re* model solutions in a number of transonic and supersonic flows involving boundary-layer separation and reattachment.

All of the above-mentioned treatments rely upon an assumed semi-logarithmic velocity and temperature distribution in the near-wall cell. To avoid these limitations, Smith [57] developed a novel wall function in conjunction with a two-equation $k-kl$ model. The wall function used simplified boundary-layer transport equations for momentum, turbulent kinetic energy and internal energy, neglecting convection and assuming a parabolic turbulent length scale profile. These transport equations were solved numerically with two or three iterations per main iteration of the solution process. The approach was shown to perform well in a flat-plate flow, transonic and supersonic flows, and a hypersonic boundary layer flow involving separation and heat transfer. Boyer & Laurence [58] also developed a wall function which avoided assumptions of local equilibrium. Their approach used shape functions to represent the velocity, k and ε distribution across the near-wall cell. These shape functions consisted of the Reichard law for velocity and profiles to match channel-flow DNS data for turbulence parameters, combined with four wall scaling factors. The scaling factors were evaluated by solving equations for the mean-flow energy and turbulent kinetic energy, incorporating terms for pressure gradient, production, destruction, diffusion and convection. The wall function was shown to reproduce channel flow profiles for a range of near-wall cell sizes ($2.5 < y^+ < 100$) but the approach has yet to be applied in more complex flows.

A rather different scheme to traditional wall functions was developed in the mid-eighties at UMIST. The Parabolic SubLayer (PSL) approach [59, 60], employed a low-Reynolds-number model using a fine near-wall grid but assumed the static pressure distribution to remain constant in a thin layer adjacent to the wall. The pressure-correction algorithm was not solved in the near-wall cells and instead the wall-normal velocity was calculated from continuity. Significant savings were reported in computing times compared to full low-*Re* solutions and results were encouraging but the approach encountered difficulties in complex geometries with the calculation of velocity in corner cells.

Efforts at UMIST have recently been focussed on two new and independent wall treatments. These share some features of the numerical wall function of Smith, described above, and the LES wall function of Balaras *et al.* (see below). The first treatment is based on the analytical integration of the momentum and energy equations, accounting for the effects of convection, pressure gradient and buoyancy forces [61]. Inevitably, fairly simple prescriptions of turbulent viscosity have to be made to allow an analytical integration, but encouraging results have been obtained for forced and mixed convection flows in pipes and an opposed-jet flow involving buoyancy effects. The second treatment is the subject of this thesis and is based on the efficient one-dimensional numerical integration of simplified low-*Re* model equations across an embedded grid within the near-wall cell.

LES Wall Functions

In LES, as in RANS, there have been different approaches to modelling the near-wall flow. The most accurate approach (which Spalart [6] refers to as “Quasi-DNS”) uses fine grid-spacing in all three

coordinate directions to resolve the near-wall turbulent streaks. This involves huge computational costs and cannot be used routinely in LES calculations. Most calculations therefore employ a coarser grid and calculate the wall shear stress for the near wall cell using a variant of the log-law (see for example [62]). A notable exception is the wall function of Balaras *et al*. [63] which is mentioned here as it shares some similarities to the RANS treatment presented in this thesis. In the Balaras *et al*. wall function, an embedded grid is defined between the near-wall node and the wall. Simplified boundary-layer-type transport equations for the wall-parallel momentum are solved numerically across the embedded grid, using a mixing-length model for the eddy-viscosity, with modified van Driest damping. The velocity profiles obtained across the embedded grid are used to provide the main LES calculation with values of the instantaneous wall shear stress. Promising results were obtained by Balaras *et al*. using this treatment for plane channel, square duct and rotating channel flows with a modest computational overhead of 10-15% compared to existing log-law treatments.

1.5 Study Objectives

The objective of the work presented in this thesis is to develop and test a new wall function for flow calculations using RANS turbulence models. The ideal properties of the wall function are as follows:

- **Accuracy**: the wall function should be practically as accurate as a low-Reynolds-number model. One cannot expect it to improve upon low-*Re* model predictions without embodying more physics or empiricism.

- **Computational Speed**: current wall functions decrease the computing time by roughly an order-of-magnitude compared to low-*Re* calculations[8]. There needs to be a significant time advantage in using the new wall function over low-*Re* treatments although probably the best one could hope for would be to equal the current status quo.

- **Robustness**: the wall function should not impair the numerical stability of the calculation.

- **Flexibility**: bearing in mind the wide variety of flows in which industrial users are interested, the wall function should be able to be adapted easily to work with different turbulence models, to include heat and mass transfer effects and to work in complex geometry.

- **Ease of Use**: it should be conceptually easy to understand and simple to implement. It should also follow as closely as possible the format of existing wall functions to make it straightforward to switch from standard wall functions to the new treatment.

[8]The saving in computing time one can achieve in switching from a low-*Re* model approach to using wall functions depends upon many factors. The most significant of these is the number of walls compared to the domain size. The stated figure of an "order-of-magnitude" decrease in computing time is based on a flow involving a single wall, such as the impinging jet flow, discussed later. In flows involving a larger number of walls for the same domain size one would expect to see a greater decrease in computing time.

- **Validation**: It is easy to make coding mistakes and, if possible, there should be simple routes to validating the wall function code.

In order to test the performance of the new wall function, a variety of flows are studied: channel, impinging jet, spinning disc and simplified car-body flows. The final flow around the "Ahmed" car body is a demanding test-case both in terms of implementation and performance: the wall function has to be coded to suit a three-dimensional non-orthogonal multiblock grid arrangement while the flow involves impingement, strong streamline curvature, separation and possibly reattachment. The Ahmed body flow is recognized as an important test-case and has been the subject of two ERCOFTAC workshops[9].

In each of the flows examined, the performance of the new wall function is compared to that of standard wall functions and low-*Re* model treatments (with the exception that the Ahmed body is not considered using low-*Re* models because the computing resources for such a calculation are currently unavailable). Computing times are also compared for each of the treatments in each of the flows.

A secondary objective of the current work is to examine the performance of the two-equation NLEVM of Craft *et al*. [30]. This has previously been tested in impinging flows by Suga [34] but for slightly different geometry. Robinson [35] also tested the NLEVM in a variety of complex flows, including the Ahmed body flow, although his study did not employ the new wall function.

1.6 Outline of Thesis

The RANS equations and "standard" wall functions used in the numerical simulations are first presented in Chapter 2. Following this, in Chapter 3, the main features of the two CFD codes used in the current study, TEAM and STREAM, are presented. Chapter 4 introduces the new subgrid-based wall function. The assumptions used in its derivations are first presented, followed by an overview of the transport equations, its implementation and finally some comments on the validation of the wall function in a simple channel flow. The following three chapters then present the test cases to which the new wall function has been applied: the impinging jet, the spinning disc and the Ahmed body flows. Each of these chapters begins with an introduction and a review of previous simulations, before going on to present results and comparisons of the new wall function's performance. The main findings of the thesis are summarized in Chapter 8.

A significant proportion of this thesis consists of appendices. The first appendix presents the full set of transport equations used in axisymmetric swirling flow. This is followed by an appendix giving a general introduction to non-orthogonal curvilinear coordinates. This introduction has been included since most undergraduate and even post-graduate courses in fluid mechanics avoid the complexity of covariant and contravariant tensor analysis, which is used to derive the RANS equations in

[9] the 9th ERCOFTAC-IAHR-COST Workshop on Refined Turbulence Modelling, Darmstadt, Germany, October 4-5, 2001 and 10th ERCOFTAC-IAHR-QNET/CFD Workshop on Refined Turbulence Modelling, Poitiers, France, October 10-11, 2002.

non-orthogonal curvilinear coordinates. It is the author's experience that textbooks on the subject are also not, in general, accessible and different notation is often used in different texts. After this introduction, Appendix C presents the RANS equations in curvilinear coordinates, where velocity vectors are aligned to the curvilinear coordinate axes. The UMIST-*N* wall function transport equations in curvilinear coordinates are then presented in Appendix D. Appendix E describes the implementation of the UMIST-*N* wall function in the STREAM code. Appendix F presents the main-grid transport equations solved in STREAM. Finally, Appendix G discusses a number of routes which have been investigated in the course of developing the new wall function which, for one reason or another, have been found not to work. This information has been included in order to fully document the work, to help explain the current choice of options used in the wall function and to serve as a guide to its future development.

Figures have been included in amongst the text where possible so that the reader does not have to continually flick between pages. However, most computational grids and results have been placed in a *Figures* section at the end of the thesis to avoid the text being split over many pages.